High-Energy Cathode Materials (Li_2MnO_3–$LiMO_2$) for Lithium-Ion Batteries

ARTICLE *in* JOURNAL OF PHYSICAL CHEMISTRY LETTERS · MARCH 2013

Impact Factor: 7.46 · DOI: 10.1021/jz400032v

2 AUTHORS:

Haijun Yu
National Institute of Advanced Industrial Scie…
44 PUBLICATIONS **765** CITATIONS
SEE PROFILE

Haoshen Zhou
National Institute of Advanced Industrial Scie…
275 PUBLICATIONS **9,884** CITATIONS
SEE PROFILE

THE JOURNAL OF PHYSICAL CHEMISTRY Letters

Perspective

pubs.acs.org/JPCL

High-Energy Cathode Materials (Li_2MnO_3–$LiMO_2$) for Lithium-Ion Batteries

Haijun Yu[†] and Haoshen Zhou*[,†,‡]

[†]Energy Technology Research Institute, National Institute of Advanced Industrial Science and Technology (AIST), Umezono 1-1-1, Tsukuba, 305-8568, Japan

[‡]National Laboratory of Solid state Microstructures & Department of Energy Science and Engineering, Nanjing University, Nanjing 210093, China

ABSTRACT: Lithium-rich layered oxide materials $xLi_2MnO_3\cdot(1-x)LiMO_2$ (M = Mn, Ni, Co, Fe, Cr, etc.) have attracted much attention for the use of cathode materials in lithium-ion batteries in recent years. However, there are many issues still unclear (the structure and reaction mechanism are ambiguous until now), and numerous scientific challenges (low initial Coulombic efficiency, poor rate capability, and voltage degradation during cycling) of these materials that must be overcome to realize their utilization in commercial lithium-ion batteries. This Perspective focuses on the challenges and prospects associated with the current researching results of these lithium-rich layered cathode materials. Specifically, their average/local structures, reaction mechanisms, and electrochemical properties are discussed.

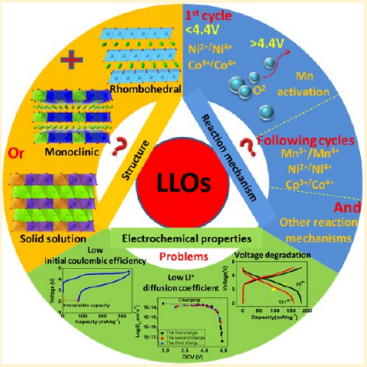

As the problems of fossil energy exhaustion, global warming, and environment pollution plague modern society, sustainable energies have gradually become a world-wide topic. There have also been increasing demands for wind or solar power stations and low-emission or zero-emission electric vehicles. Lithium-ion batteries are of great significance as power sources to satisfy these demands and realize a low-carbon society.[1−5] However, the energy density of current lithium-ion batteries is still not enough for market requirements, and their cost and environment-related issues should be also considered for much broader market penetration.[6,7]

Owing to the key roles of cathode materials on energy density and the cost of current lithium-ion batteries, several alternative cathode materials, such as $LiCoO_2$, $LiNi_{0.8}Co_{0.15}Al_{0.05}O_2$, $LiNi_{0.33}Co_{0.33}Mn_{0.33}O_2$, spinel $LiMn_2O_4$, olive $LiFePO_4$, and so on, have been commercially used in lithium ion batteries.[3,4] However, the available rechargeable capacity for all of these materials almost approaches their limits (120−200 mAh/g), thus cathode materials associated with higher specific capacity are needed to meet the demand for further energy density enhancement of lithium-ion batteries. During the past two decades, much effort on exploiting new cathode materials has been done (Figure 1).[3,7−10]

Among the reported cathode materials so far, the lithium-rich layered oxide materials (LLOs) have attracted much attention in recent years because their capacities can be larger than 280 $mAhg^{-1}$ with 3.6 V or larger operating voltages when these materials are charged to over 4.6 V at room temperature.[11−15] These LLOs can be described with two completely different notations: $xLi_2MnO_3\cdot(1-x)LiMO_2$ (M = Mn, Ni, Co, Fe, Cr, etc.) and $Li_{1+(x/(2+x))}M'_{1-(x/(2+x))}O_2$ (M′ = Mn+M). Both

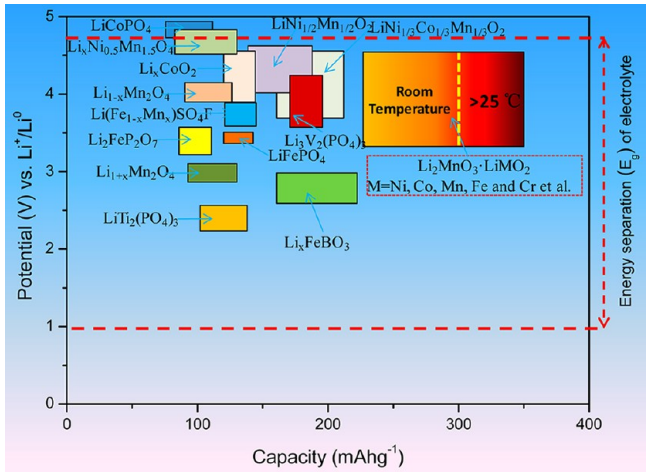

Figure 1. Voltage and capacity of the main cathode materials for lithium-ion batteries.

notations are equal to the same material and have been used extensively in the published literature. For example, the $0.5Li_2MnO_3\cdot0.5LiMn_{0.42}Ni_{0.42}Co_{0.16}O_2$ material can also be described as $Li[Li_{0.2}Mn_{0.567}Ni_{0.166}Co_{0.067}]O_2$.[13−15] In this Perspective, we will focus on the challenges and prospects of these LLOs with three sections for the next-generation lithium-ion batteries. In the first section, the design theory and average/

Received: January 7, 2013
Accepted: March 28, 2013
Published: March 28, 2013

local structures are discussed. The second section discusses the reaction mechanisms, especially the first charge and discharge processes. The third section describes the electrochemical performance, current main problems, and improving methods of these LLOs.

The rechargeable capacity and energy density of LLO materials at room temperature can be close to 280 $mAhg^{-1}$ and 1000 $Whkg^{-1}$, respectively, which are about twice that of current commercial cathode materials for lithium ion batteries.

These LLOs were first researched as cathode materials for rechargeable lithium batteries by Thackeray et al. when they were researching the $LiMnO_2$ layered materials.[16,17] In 1991, inspired by Hunter's discovery that acid treatment of the spinel $LiMn_2O_4$ yielded λ-MnO_2 with a Mn_2O_4 spinel framework, Thackeray et al. synthesized the layered lithium−manganese oxide compound $Li_{2-x}MnO_{3-x/2}$ ($0 < x < 2$) with a cubic-close-packed oxygen anion array by chemical leaching of Li_2O from the rock salt phase Li_2MnO_3 ($Li_2O{\cdot}MnO_2$) with acid at 25 °C, and got the compound $Li_{1.09}Mn_{0.91}O_2$ or $0.2Li_2MnO_3{\cdot}0.8LiMnO_2$ after relithiation in an electrochemical cell.[16,17] The structure stability of this compound is much better than that of the pure layered $LiMnO_2$ cathode material during electrochemical cycling, and then the $xLi_2MnO_3{\cdot}(1-x)LiMnO_2$ material concept is first introduced. When Kalyani et al. first found that the monoclinic Li_2MnO_3 material could be activated electrochemically by charging the Li/Li_2MnO_3 cell to 4.5 V, the $xLi_2MnO_3{\cdot}(1-x)LiMO_2$ (M = Mn, Ni, Co, Fe, Cr, etc.) materials became more and more attractive.[18] This notation can not only describe the electrochemical processes of these LLOs combining with the single $LiMO_2$ (M = Mn, Ni, Co, Fe, Cr, etc.) and Li_2MnO_3 component electrochemical process, but also indicates that the cathode materials for lithium

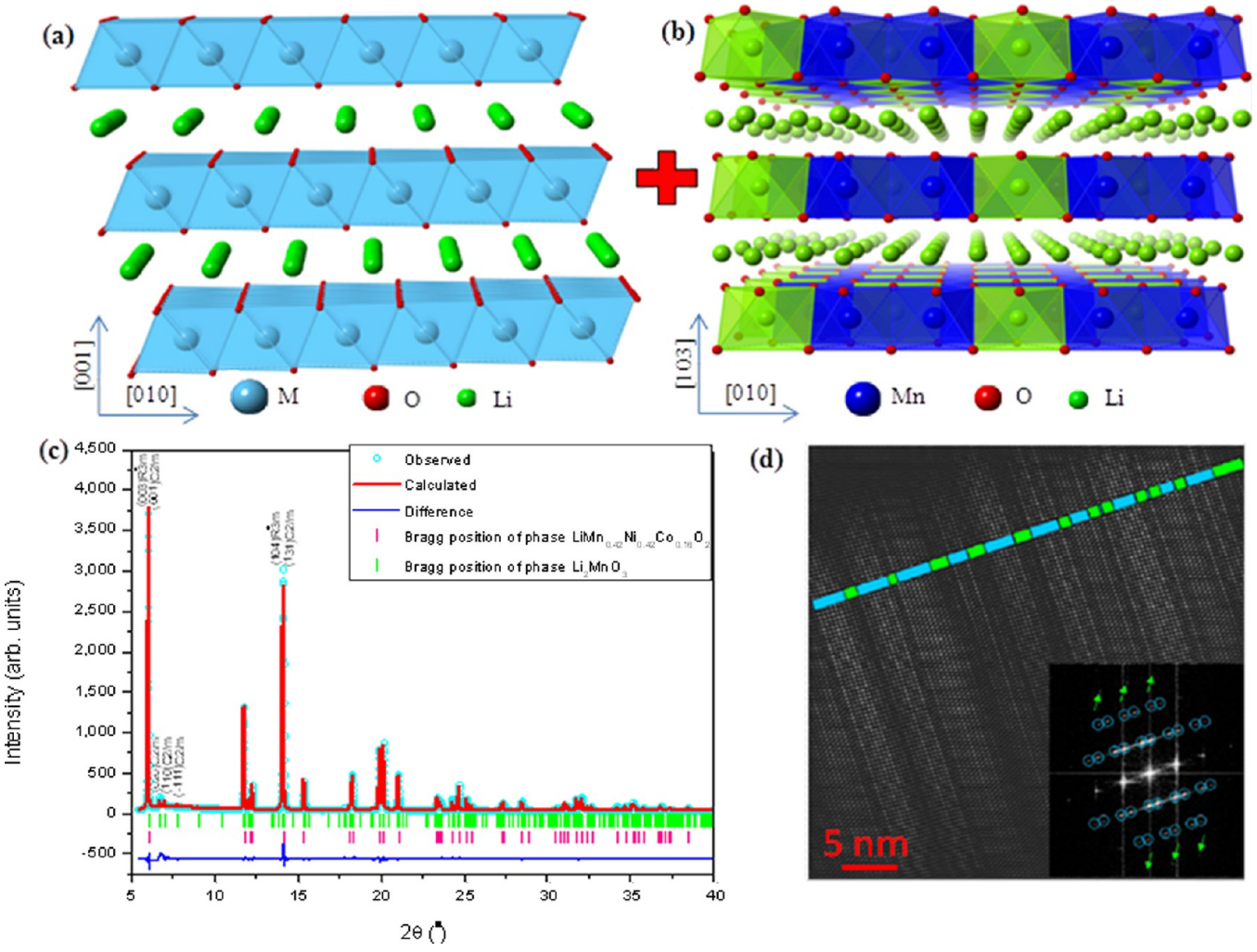

Figure 2. Crystal structure of the (a) rhombohedral $LiMO_2$ structure (space group: $R\bar{3}m$, M = Ni, Co, Mn, Fe, Cr, etc.) and (b) monoclinic Li_2MnO_3 structure (space group: $C2/m$) viewed from the [100] crystallographic direction. (c) Synchrotron powder X-ray diffraction pattern and Rietveld refinement profile of the $0.5Li_2MnO_3{\cdot}0.5LiMn_{0.42}Ni_{0.42}Co_{0.16}O_2$ material with rhombohedral and monoclinic structures. Reprinted with permission from ref 13. Copyright 2012 Royal Society of Chemistry. (d) Bragg filtered high-angle annular dark field scanning transmission electron microscopy (STEM-HAADF) image of the $Li_{1.2}Mn_{0.61}Ni_{0.18}Mg_{0.01}O_2$ material, containing Li_2MnO_3 parts (blue) and $LiNi_{0.45}Mn_{0.525}Mg_{0.025}O_2$ ones (green). Reprinted with permission from ref 33. Copyright 2012 American Chemical Society.

dx.doi.org/10.1021/jz400032v | J. Phys. Chem. Lett. 2013, 4, 1268−1280

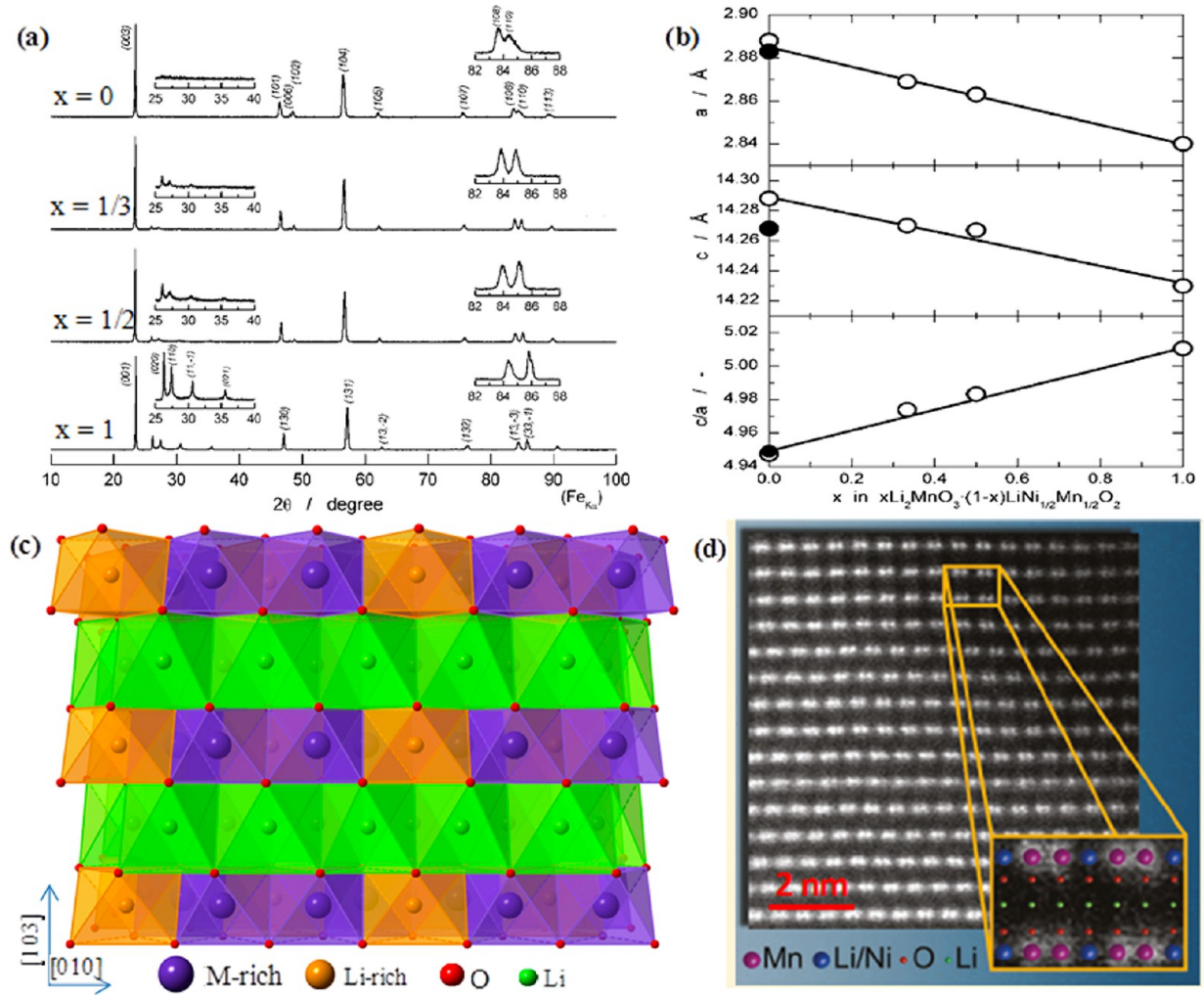

Figure 3. (a) XRD patterns and (b) hexagonal lattice parameters of the $xLi_2MnO_3{\cdot}(1-x)LiNi_{1/2}Mn_{1/2}O_2$ (x = 0, 1/3, 1/2, and 1) materials. Reprinted with permission from ref 40. Copyright 2012 Royal Society of Chemistry. (c) Homogeneous solid solution structure with partial ordered $C2/m$ monoclinic phase viewed from the [100] crystallographic direction. (d) Aberration-corrected scanning transmission electron microscopy (STEM) image of the $Li[Li_{0.2}Ni_{0.2}Mn_{0.6}]O_2$ crystal. Reprinted with permission from ref 37. Copyright 2011 American Chemical Society.

ion batteries can be designed with different contents of $LiMO_2$ (M = Mn, Ni, Co, Fe, Cr, etc.) and Li_2MnO_3 components, realizing the variational electrochemical performances (rechargeable capacity, rate performance, and cycle stability) of lithium ion batteries.[11,19−24] Following this materials designation proposition, many other composite materials between Li_2NO_3 (N = Mn, Ti, and Zr) and layered $LiMO_2$ (M = Mn, Ni, Co, Fe, Cr, etc.) or spinel $LiMn_2O_4$ have also been proposed and researched during the past decade.[25−28] Among them, these LLOs are hot topics of research for their high energy density and low cost.

Owing to the importance of the relationship between the structure and electrochemical performance of electrode materials for lithium-ion batteries, it is necessary to reveal the actual structure of these LLOs to deeply understand and precisely control their electrochemical performance. Until now, there has been an ongoing debate in the literature on whether these LLOs form homogeneous solid solutions or Li_2MnO_3 domains within a $LiMO_2$ matrix.[3,20,27,29−42] In this Perspective, first, we will discuss the pristine structures of these LLOs based on the average and local structures analysis.

Figure 2a,b shows the rhombohedral $LiMO_2$ structure (space group: $R\bar{3}m$, M = Co, Ni, Mn, Fe, Cr, etc.) and monoclinic Li_2MnO_3 structure (space group: $C2/m$) viewed from their [100] crystallographic direction, respectively. As the Li_2MnO_3 structure can be reformulated with $Li[Li_{1/3}Mn_{2/3}]O_2$, the monoclinic Li_2MnO_3 structure is very similar to the rhombohedral $LiMO_2$ structure, and can be considered as a particular case of $LiMO_2$ with an M layer consisting of a periodic sequence of one Li and two Mn atoms. Thus, both of these two structures can be considered layered α-$NaFeO_2$-type rock salt structures, and all the octahedral sites of their close-packed oxygen arrays are occupied. The experimental synchrotron X-ray diffraction (SXRD) patterns of the LLO ($0.5Li_2MnO_3{\cdot}0.5LiMn_{0.42}Ni_{0.42}Co_{0.16}O_2$) is shown as the cyan circles in Figure 2 c.[13] It is clear that all peaks can be well indexed on the basis of $LiNiO_2$ structure with a space group $R\bar{3}m$ except for those weak peaks around 6.4−8°. These peaks can be indexed to the (020), (110), and ($\bar{1}$11) lattice planes of a Li_2MnO_3-like unit cell with monoclinic ($C2/m$) symmetry, indicating the existence of Li_2MnO_3-like phase structure. On the basis of the Rietveld structure refinement of this material with different models by the RIETAN-FP program, the whole diffraction pattern, including the weak peaks around 6.4−8°, can be refined well if the two-phase model consisting of rhombohedral $LiMn_{0.42}Ni_{0.42}Co_{0.16}O_2$ (space group $R\bar{3}m$) and

dx.doi.org/10.1021/jz400032v | J. Phys. Chem. Lett. 2013, 4, 1268−1280

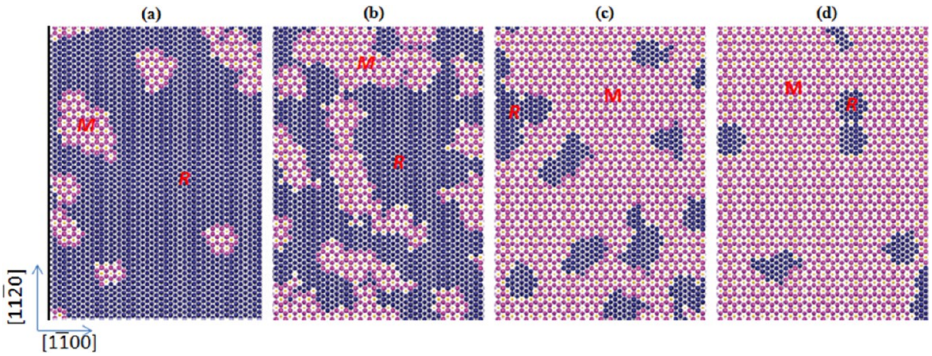

Figure 4. The expected morphology evolution of the TM plane in $x\mathrm{Li_2MnO_3}\cdot(1-x)\mathrm{LiCoO_2}$, showing the coexistence of Co and $\mathrm{LiMn_2}$ domains: (a) $x = 0.15$; (b) $x = 0.45$; (c) $x = 0.75$; and (d) $x = 0.90$. The rhombohedral (R) and monoclinic (M) unit cells are indicated in the figure. Reprinted with permission from ref 29. Copyright 2011 American Chemical Society.

monoclinic $\mathrm{Li_2MnO_3}$ (space group $C2/m$) structures are chosen. The phase fractions of the rhombohedral and monoclinic components are 43% and 57%, respectively, and very close to the composition of the studied $0.5\mathrm{Li_2MnO_3}\cdot0.5\mathrm{LiMn_{0.42}Ni_{0.42}Co_{0.16}O_2}$ material.[13]

By the high-resolution transmission electron microscopy (HRTEM) technique combined with electron energy-loss spectroscopy (EELS) technique, Wen, Abraham, Tabuchi et al. find that the locally monoclinic ($\mathrm{Li_2MnO_3}$-like) regions are existed in the parent rhombohedral structure of these LLOs,[22,29,31,36] and there are obvious Mn-rich nanodomains.[22,32,43] The recent research on these LLOs by high-angle annular dark field scanning transmission electron microscopy (HAADF-STEM) also reveals the coexistence of two phases inside the $\mathrm{Li_{1.2}Mn_{0.61}Ni_{0.18}Mg_{0.01}O_2}$ ($0.6\mathrm{Li_2MnO_3}\cdot0.4\mathrm{LiNi_{0.45}Mn_{0.525}Mg_{0.025}O_2}$) material; the $C2/m$ structure with accentuated contrast slab and the $R\bar{3}m$ structure with attenuated contrast slab are encountered in the blue and green parts (Figure 2d), respectively, and the proportion of these two structures are about 55% and 45%, respectively, which is in agreement with the component composition of their studied material.[33] In addition, both extended X-ray absorption fine structure (EXAFS) and Li magic-angle spinning (MAS) nuclear magnetic resonance (NMR) spectroscopy techniques studies on these LLOs also state that most $\mathrm{Mn^{4+}}$ in $\mathrm{Li_2MnO_3}$-like atomic environments and $\mathrm{M^{n+}}$ in $\mathrm{LiMO_2}$-like (M = Co, Ni, Mn, Fe, Cr; $2 \le n \le 4$) atomic environments are contained inside these LLOs, and the locally monoclinic $\mathrm{Li_2MnO_3}$-like structures are probably quasi-random distributed within the rhombohedral α-$\mathrm{NaFeO_2}$ framework.[27,29,38,39]

Although there is much two-phase evidence of these LLOs by average and local structure studies, on the other hand, some researchers think that these LLOs are homogeneous solid solutions between the two components $\mathrm{Li_2MnO_3}$ and $\mathrm{LiMO_2}$ (M = Co, Ni, Mn, Fe, Cr), because their lattice parameters vary linearly with the composition of its end members (Figure 3 b).[20,35,37,40] This indicates that these samples follow Vegard's rule. These weak peaks around 25−35° (XRD data) are also proposed as the result from long-rang Li ordering with a $\sqrt{3}a_{hex} \times \sqrt{3}b_{hex}$ superstructure in the transition-metal layer (Figure 3 a).[35] Note that, although some researchers take the solid solution opinion, the crystal symmetries of these LLOs are also being debated. Some researchers consider these LLOs as being composed of a solid solution with $R\bar{3}m$ rhombohedral symmetry,[20,35] while others indicate that these LLOs belong to a solid solution with $C2/m$ monoclinic symmetry.[37] It is worth noting that the X-ray diffraction techniques (XRD or SXRD) can only provide key information on the average crystal structure. As a matter of fact, the large difference between the atomic number, size, and tendency for like or unlike atom clusters of the elements (Li, Mn, Ni, Co, Fe, Cr) inside these LLOs can induce large lattice distortions, although these LLOs can preserve the periodical long-range structure. There are many examples of multistructural phases existing inside one material although their long-range structures can be considered a solid solution.[29,44,45]

Thus, the local structure studies on these LLOs are very important to investigate their actual structure. Jarvis et al. carefully investigated the $\mathrm{Li[Li_{0.2}Ni_{0.2}Mn_{0.6}]O_2}$ material with a diffraction scanning transmission electron microscopy (D-STEM) technique, and indicated that this material formed a partial ordered solid solution (Figure 3c,d).[37] At the same time, they also concluded that, although two phases have not been observed for their studied material, other compositions, especially those with less excess lithium, may result in two-phase regions.[37] For $\mathrm{Li_2MnO_3}$ material, there is no doubt that this material has been evidenced as the monoclinic structure with $C2/m$ space group.[46] The ratio of Li and Mn content inside this material is 2. In particular, there are about 0.33 Li and 0.67 Mn atoms located at the monoclinic ordering of $\mathrm{LiMn_2}$ planes with Li−Mn−Mn periodic arrangement. For $\mathrm{Li[Li_{0.2}Mn_{0.567}Ni_{0.166}Co_{0.067}]O_2}$, $\mathrm{Li[Li_{0.2}Co_{0.4}Mn_{0.4}]O_2}$, or other LLOs associated with less lithium, the composition of these materials can be described as the common formulation $\mathrm{Li[Li_xM_{1-x}]O_2}$ (M = Mn, Ni, Co, etc.; $x < 0.33$).[13,29,36] It is obvious that there are not enough lithium sources to support the overall $\mathrm{LiM_2}$ periodic ordering. Therefore, two-phase domains with M−M (M = Mn, Ni, Co, Fe, and Cr) and Li−M′−M′ (M′ = Mn, etc.) periodic ordering in local regions most probably exist inside these LLOs when their compositions are located between the $\mathrm{LiMO_2}$ (M = Mn, Ni, Co, Fe, and Cr) and $\mathrm{Li_2MnO_3}$ components. Experiments by Dahn et al. also confirmed that more and more Li atoms occupied the Ni and Mn layer with the increase of y at fixed $x = 1.1$ for the $\mathrm{Li_xMn_yNi_xO_2}$ ($0.9 \le x \le 1.2$; $0.1 \le y \le 0.5$) material, the solid solution series $\mathrm{Li_xMn_yNi_xO_2}$ as a single phase could only be prepared for x near 1 and $0 \le y \le 0.5$, and more impurities (especially $\mathrm{Li_2MnO_3}$) were shown with more larger y ($y = 0.6$).[47] In addition, the raw materials, preparation methods, and calcination temperatures are also the important influence factors for determining the structure of these LLOs with homogeneous solid solution or two phases. Therefore, the

dx.doi.org/10.1021/jz400032v | J. Phys. Chem. Lett. 2013, 4, 1268−1280

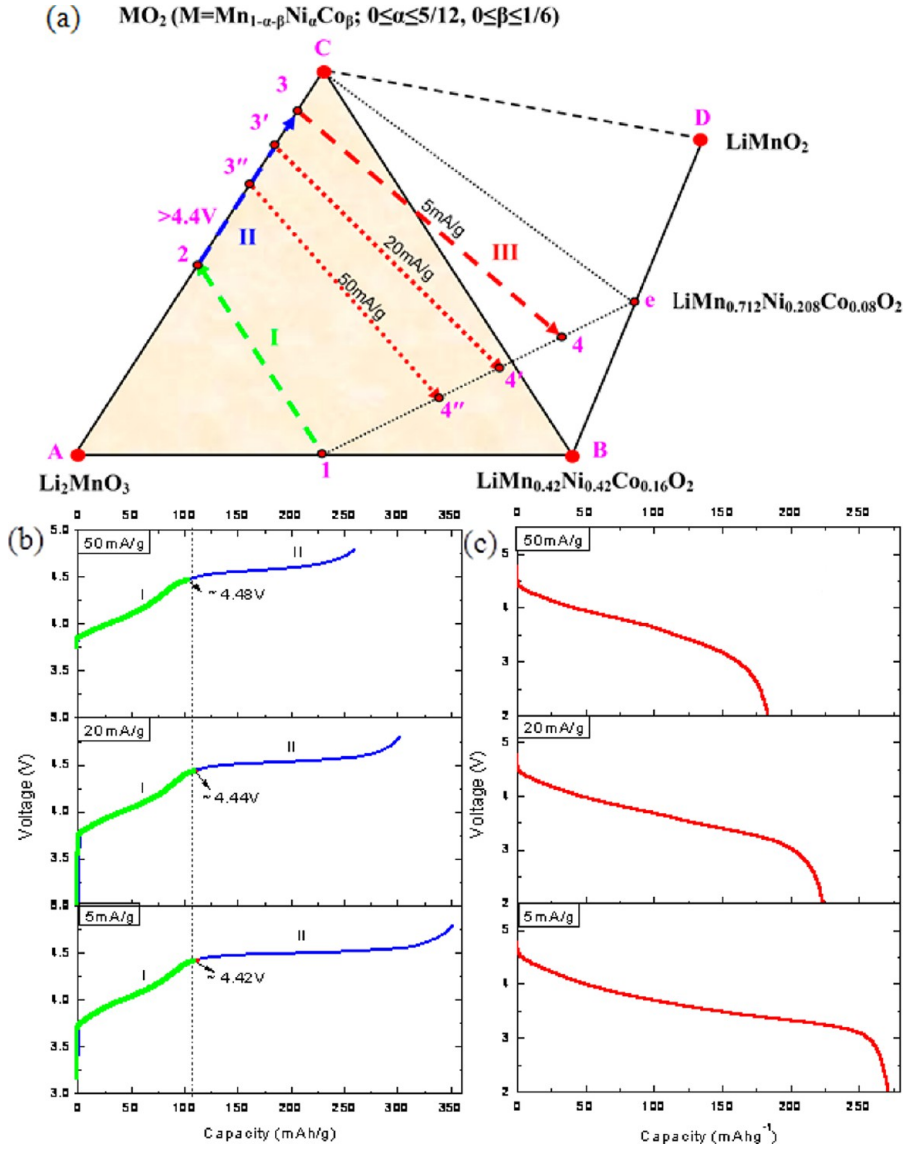

Figure 5. (a) Reaction pathways diagram through controlling the activation of the Li_2MnO_3 phase inside the $0.5Li_2MnO_3{\cdot}0.5LiMn_{0.42}Ni_{0.42}Co_{0.16}O_2$ material based on the three-dimensional compositional phase diagram. (b) The charge and (c) discharge curves with three different current densities. (a–c) Reprinted with permission from ref 13. Copyright 2012 Royal Society of Chemistry.

domains with Li_2MnO_3-like components most probably exist inside these LLOs, increased with the lithium and manganese content (in proportion to x in the $xLi_2MnO_3{\cdot}(1-x)LiCoO_2$ equation) increasing, which is described by the simulated figure in Figure 4.[29]

The reaction mechanisms of these LLOs are very complicated, and have been extensively researched and discussed in the past decade.[6,11,12,25,35,40,42,48−55] However, these reaction mechanisms proposed are still being debated, and most of them cannot explain all of the electrochemical phenomena or are merely supposition.

In order to understand the complex electrochemical or chemical reaction processes during the first and following cycles of these LLOs, one of the reaction mechanisms associated with an integrated three-dimensional compositional phase diagram (Figure 5a) is introduced based on Thackeray's two-dimensional phase diagram and our previous structure studies of these LLOs.[13] Following this phase diagram, the reaction pathways, phase composition change, and the reaction mechanism of these LLOs during lithium extraction and insertion processes can be well explained.

For the $0.5Li_2MnO_3{\cdot}0.5LiMn_{0.42}Ni_{0.42}Co_{0.16}O_2$ electrode material, the reaction pathways and phase composition changes during the first charge region below 4.4 V with different current densities vary along the green lines in Figure 5a,b, from point 1 to point 2. During this period, maximum 0.5 Li^+ ions can be extracted from the lithium layer of the $0.5LiMn_{0.42}Ni_{0.42}Co_{0.16}O_2$ component associated predominantly with the oxidation of nickel ions from Ni^{2+} to Ni^{4+} and followed by the trivalent cobalt oxidation process at higher voltage. The practical charge capacity is 111, 108, and 103 mAh/g, respectively, associated with 5, 20, and 50 mA/g initial current density at room temperature, which is a little smaller than the theoretical capacity (126 mAh/g, assuming all the nickel and cobalt are oxidized to tetravalent).

When the electrochemical potential of the Li/$0.5Li_2MnO_3{\cdot}0.5LiMn_{0.42}Ni_{0.42}Co_{0.16}O_2$ cell increases from 4.4 to 4.8 V during the first charge process, presented with the blue

dx.doi.org/10.1021/jz400032v | J. Phys. Chem. Lett. 2013, 4, 1268−1280

long voltage plateaus in Figure 5 b, more lithium ions can be extracted from the Li_2MnO_3 component together with the loss of oxygen and structure rearrangement, and there is probably a new phase (MnO_2) formed. The oxygen accompanied with lithium ions extraction and structure rearrangement phenomena during this process have been confirmed by Armstrong using in situ differential electrochemical mass spectrometry (DEMS) (Figure 6a), Yabuuchi using SXRD, and Lu using Rietveld analysis.[50,52,56] It is clear that the evolution of oxygen gas quantity in Figure 6a is associated with the voltage increasing, and the large amount of oxygen gas is emitted above 4.5 V, corresponding to the charge plateau of these LLOs. Through first-principles calculations, the oxygen 2p electron clouds change significantly with the lithium extraction during the first charge process, indicating that extra electrons that cannot be provided by the transitional metal redox couples are coming from oxygen ions (Figure 6b–e).[34] However, it is very difficult to unambiguously determine whether the new phase is MnO_2, although new phases created during the first charge process have been reported by Simonin and Gray in $Li[Li_{0.2}Mn_{0.61}Ni_{0.18}Mg_{0.01}]O_2$ and $Li[Li_{1/9}Ni_{1/3}Mn_{5/9}]O_2$ materials, respectively.[57,58] In our opinion, based on electrochemical performances, dQ/dV curves and kinetic analysis of these LLOs during cycling, the new phase (MnO_2) is most likely to appear during the first charge process above 4.4 V, and transfer to the cubic spinel-like framework ($MnMO_4$, M = Ni, Co, and Mn) during the following cycles.[13,15] The theoretical capacity of this process (from 4.4 V to 4.8 V) is calculated to be 251 mAh/g if we suppose all of the lithium (0.5 Li_2O) can be extracted from the $0.5Li_2MnO_3$ component. The practical charged capacities of this process are 205, 162, and 139 mAh/g, respectively, corresponding to different current densities (5, 20, and 50 mA/g) at room temperature. All of the practical charged capacities are close but smaller than those of theoretical capacity. Thus, the reaction pathways and compositional changes of this process at room temperature can be described with the blue lines in Figure 5a, from point 2 to points 3, 3′, and 3″, respectively. During these charge regions, when all of Li_2O are extracted from the Li_2MnO_3 component, the oxidized electrode material will be $Mn_{0.712}Ni_{0.208}Co_{0.08}O_2$ with $\alpha = 0.208$ and $\beta = 0.08$ in MO_2 ($M = Mn_{1-\alpha-\beta}Ni_\alpha Co_\beta$; $0 \le \alpha \le 5/12$, $0 \le \beta \le 1/6$), and the electrode composition changes along the blue dashed line until it reaches the apex C of the tie-triangle in Figure 5a.

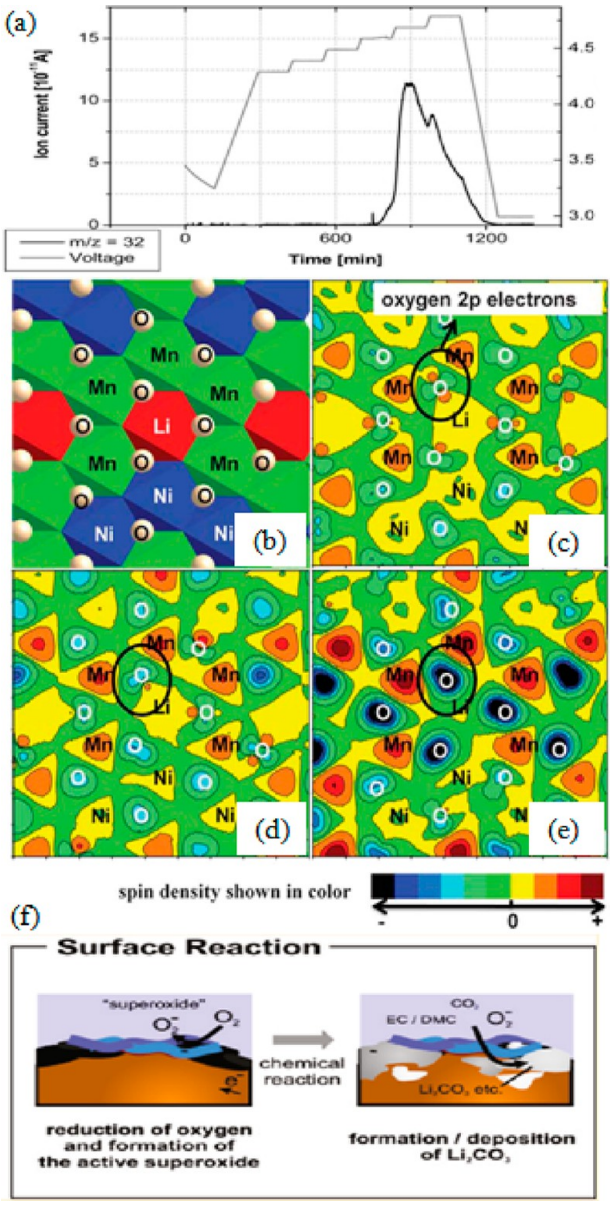

Figure 6. (a) Mass spectrometry analysis of O_2 evolved on the 1st charging process of the $Li/Li[Ni_{0.2}Li_{0.2}Mn_{0.6}]O_2$ cell. Reprinted with permission from ref 52. Copyright 2006 American Chemical Society. (b) First-principle calculation sketch of partial oxygen layer in $Li_{x/14}Ni_{1/4}Mn_{7/12}O_2$ (pink balls: oxygen ions; colored polyhedrons: adjacent *TM* slab) and its calculated spin density at (c) $x = 14$, (d) $x = 8$, and (e) $x = 0$. Reprinted with permission from ref 34. Copyright 2011 Royal Society of Chemistry. (f) Schemes of the proposed surface reaction mechanisms in the $Li_{1.2}Ni_{0.13}Co_{0.13}Mn_{0.54}O_2$ material. Reprinted with permission from ref 50. Copyright 2011 American Chemical Society.

> The reaction mechanisms associated with the mysterious anomalous capacity of these LLOs at high temperature may be different compared with those at room temperature, and are still unclear.

During the first discharge process, lithium ions will insert into the $Mn_{0.42}Ni_{0.42}Co_{0.16}O_2$ and newly formed MnO_2 components, respectively, while the unactivated Li_2MnO_3 component still exist in these "composite" layered materials. Our previous and Yabuuchi's research results show that the activated manganese redox reaction (Mn^{3+}/Mn^{4+}) occurs after the first cycle of these LLOs.[13,50] Therefore, the electrochemical reaction pathways and composition change of the first discharge process is not suitable to be located in the Li_2MnO_3–$LiMO_2$ (M = Mn, Ni, and Co) tie-line in Figure 4 of ref 11, and should be located in the face compositing Li_2MnO_3, $LiMnO_2$, and $LiMO_2$ (M = Mn, Ni, and Co) components. The reaction pathways and compositional changes during the first discharge processes of these LLOs with different current densities can follow the red lines in Figure 5a. During this process, the theoretical discharge capacity is calculated to be 269 mAh/g based on the weight of the $0.5LiMnO_2 \cdot 0.5LiMn_{0.42}Ni_{0.42}Co_{0.16}O_2$, while the practical discharge capacity, corresponding to 5, 20, and 50 mA/g initial

dx.doi.org/10.1021/jz400032v | J. Phys. Chem. Lett. 2013, 4, 1268–1280

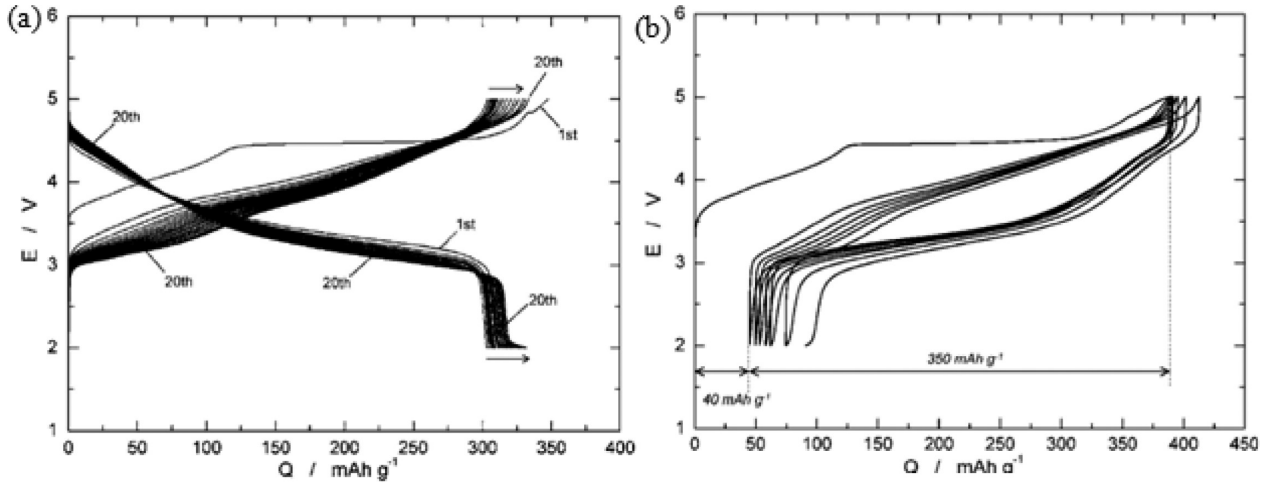

Figure 7. Charge and discharge curves of the Li/Li[$Li_{1/5}Ni_{1/5}Mn_{3/5}$]O_2 cell at (a) 55 °C and (b) 85 °C. Reprinted with permission from ref 40. Copyright 2011 Royal Society of Chemistry.

charge/discharge currents, is 272, 224, and 184 mAh/g, respectively (Figure 5c). It is obvious that all of the discharge capacity except for the value with small current density (≤5 mA/g) can be explained by the proposed reaction mechanism. On the basis of surface reaction investigation of these LLOs, it is suggested that some of the extra discharge capacity for these LLOs originated from the electrochemical reduction reaction of the oxygen molecules at the electrode surface ($O_2 \xrightarrow{\text{reduction}} O_2^-$), but these contribution are suppressed by the accumulated lithium carbonate formation at the electrode surface (Figure 6f).[50]

Nevertheless, with the temperature increased to 55 and 85 °C, the rechargeable charge/discharge capacity of the Li/Li[$Li_{1/5}Ni_{1/5}Mn_{3/5}$]O_2 can reach 300 mAh/g (Figure 7a), and even 350 mAh/g (Figure 7b), which are much larger than the theoretical capacity if we just consider the nickel (Ni^{2+}/Ni^{4+}) and manganese (Mn^{3+}/Mn^{4+}) valence variation.[40] Ozhuku et al. speculated that the highest rechargeable theoretical capacity at high temperature was contributed by the possible "cation" redox reaction (Mn^{4+}/Mn^{5+}, Mn^{5+}/Mn^{6+}) or "anion" redox (O^{2-}/O_2^{2-}) in a solid matrix in terms of lithium insertion scheme.[40] The reaction mechanism of these LLOs at high temperature may be different and more complex compared with those at room temperature, and more experimental evidence or theoretical calculations for supporting these hypotheses need to be conducted in the future to explain the high mysterious rechargeable capacity of these LLOs.

Although there are many debates on these LLOs currently, their large electrochemical capacities are still very attractive for utilization as cathode materials in lithium ion batteries. In the past, different composition, preparation methods, first or second crystalline grain morphology, surface treatments and doping elements of these LLOs have been extensively studied.[40,42,59−67] However, many problems of these LLOs still exist at present. For example, the initial coulombic efficiency is low,[14,68] and the cycle stability[13,69] and rate performance[15,62] of these materials still need to be amended to satisfy the application requirements.

Low initial Coulombic efficiency associated with large irreversible capacity can result in mass ionized lithium, and the formation of a solid electrolyte interface (SEI) layer, thus reducing the energy density of the lithium-ion battery and

Currently, the low initial coulombic efficiency, unsatisfied rate performance, and cycle stability of these LLOs are still the main problems preventing their utilization in practical lithium ion batteries.

presenting a serious trade-off in lithium-ion battery design. At present, most of the initial Coulombic efficiencies of these LLOs in the published literature are smaller than 80% at room temperature, and the main reason is due to the irreversible reaction resulting from the first charge plateau above 4.4 V. In order to improve the initial Coulombic efficiency, the preconditioned methods with NH_3 and HNO_3,[53] surface modification with nanostructured Al_2O_3, $AlPO_4$, or RuO_2,[70] and ruthenium substitution[14] for manganese on these LLOs have been conducted. The experiment results of ruthenium substitution for manganese (Figure 8) show that all of the initial columbic efficiency increased with the ruthenium content increasing, and the highest initial columbic efficiency is 86% with 284 mAh/g discharge capacity at room temperature when the content of substituted ruthenium is 5 mol %.[14] The initial Coulombic efficiency improvements are most probably contributed by the content decrease of the Li_2MnO_3 component or Li_2MnO_3 component, which can be activated inside these materials.

Although most of the published literature shows that the cycle performance based on the charge and discharge capacity of these LLOs is good, their voltage degradation after long cycling is extremely serious, which can largely lower the energy output and efficiency of the lithium-ion batteries.[69,71] In order to investigate the cycle stability of these materials in detail, long time cycling of the Li/0.5Li_2MnO_3·0.5$LiMn_{0.42}Ni_{0.42}Co_{0.16}O_2$ cell has been conducted.[13] It is obvious that two cycling stages (Stage I in Figure 9a and Stage II in Figure 9c) exist during long time cycling. During Stage I (from about the second cycle to the 25th cycle), the charge and discharge capacities (especially below 3.5 V) increase with cycling, while those decrease during Stage II (from about the 26th cycle to the

dx.doi.org/10.1021/jz400032v | J. Phys. Chem. Lett. 2013, 4, 1268−1280

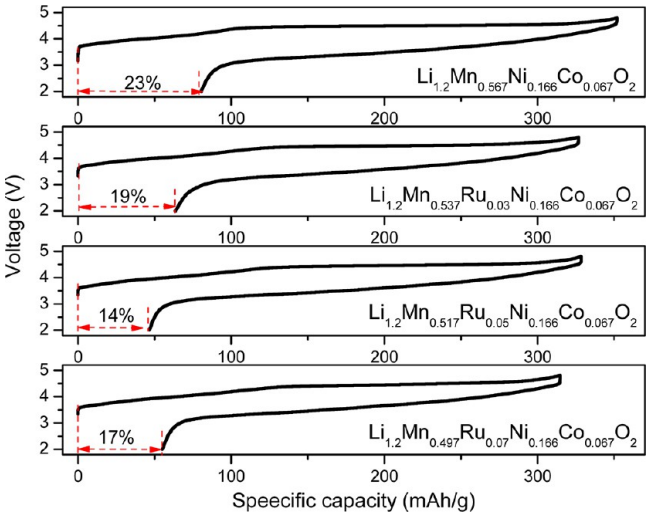

Figure 8. The initial Coulombic efficiency and the charge/discharge capacity of the $Li_{1.2}Mn_{0.567-x}Ru_xNi_{0.166}Co_{0.067}O_2$ (x = 0.00, 0.03, 0.05, and 0.07) materials. Adapted from ref 14. Copyright 2012 Royal Society of Chemistry.

151st cycle). The increased capacity in Stage I is obvious and corresponds to the new redox peaks (O_{x3}/R_{e3}) increasing after the first cycle (Figure 9b). This indicates that the content of activated manganese increases step by step during Stage I. Consequently, the charge/discharge capacity increases, and the charge voltage decreases gradually, attributed to the lower redox reaction voltage of Mn^{3+}/Mn^{4+} with respect to that of nickel and cobalt. During Stage II, both the charge/discharge capacity and discharge plateaus decrease with cycling. The decreased discharge plateaus are mostly contributed to the reduction peaks shifting to the lower voltage region (Figure 9d), indicating that the structures of these LLOs are not stable during long cycling.

Observing Figure 9b,d, we found that there are obvious swellings on the oxidation curves of dQ/dV between 3.0 and 3.2 V during Stage I, and this swelling become more and more obvious during Stage II. These phenomena indicate that the cubic spinel-like phase transformation of layered phase in local regions may arise during stage I and gradually completed during Stage II. In order to confirm these phase transformation, the Raman spectroscopies of these materials with different initial charge/discharge states were investigated. From observing Figure 9e–i, it is clear that the shoulders characterizing cubic spinel-like phase spectroscopy between 630 and 670 cm^{-1} appear and become more and more obvious with the cycle number and initial charge/discharge current density increasing. In addition, X-ray absorption spectroscopy (XAS),[55] HRTEM techniques,[33,72] and dQ/dV curves[42] studies on these LLOs also show that the cubic spinel-like phases appear after long cycling.

Surface coating with Al_2O_3, CeO_2, ZrO_2, SiO_2, ZnO, $AlPO_4$, and Li–Ni–PO_4 and mildly acidic treatment on these LLOs can enhance the cycling stability, but these coatings cannot adequately overcome the voltage decay.[53,73,74] That means that the phase transitions from layered structure into cubic spinel-like structure of these LLOs not only occurs on the particle surface, but also inside the particle bulk. As a matter of fact, the transformation of layered $Li_{0.5}MO_2$ (delithiation) into the ideal cubic spinel phase $(Li)_{8a}[M_2]_{16d}O_4$ just requires a migration of one-fourth of the transition metal ion from the octahedral sites (3b sites) of the M planes into the empty octahedral sites (3a sites) of the lithium planes and to what become 16d positions of spinel without changing the framework of closed-paced

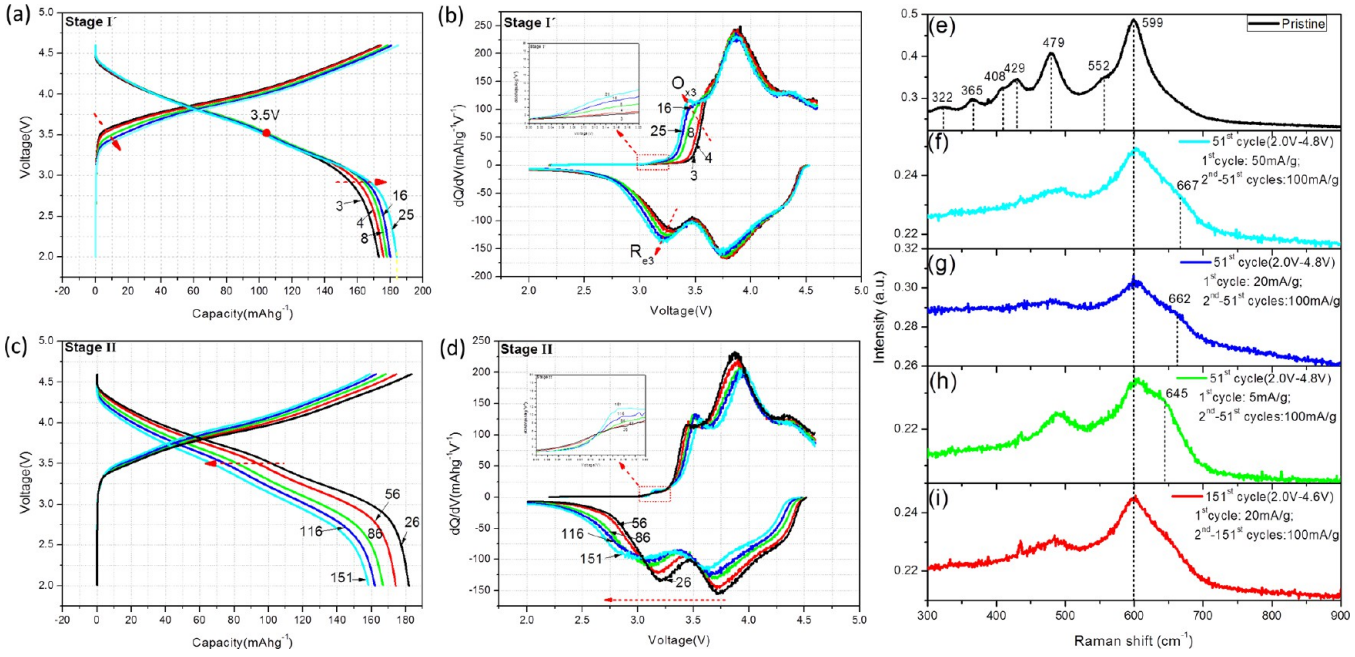

Figure 9. Charge/discharge and dQ/dV profiles at different cycling stages ((a,b), Stage I: from the 2nd cycle to the 25th cycle; (c,d), Stage II: from the 26th cycle to the 151st cycle) of the $Li/0.5Li_2MnO_3{\cdot}0.5LiMn_{0.42}Ni_{0.42}Co_{0.16}O_2$ cell. Raman profiles of the $0.5Li_2MnO_3{\cdot}0.5LiMn_{0.42}Ni_{0.42}Co_{0.16}O_2$ materials with different testing conditions: (e) pristine material; (f,g,h) electrode materials after 51 electrochemical cycles with 50 mA/g, 20 mA/g and 5 mA/g initial charge/discharge current density and 2.0–4.8 V cutoff voltage: (i) electrode material after 151 electrochemical cycles with 20 mA/g initial charge/discharge current density and 2.0–4.6 V cutoff voltage. (a–i) Reprinted with permission from ref 13. Copyright 2012 Royal Society of Chemistry.

dx.doi.org/10.1021/jz400032v | J. Phys. Chem. Lett. 2013, 4, 1268–1280

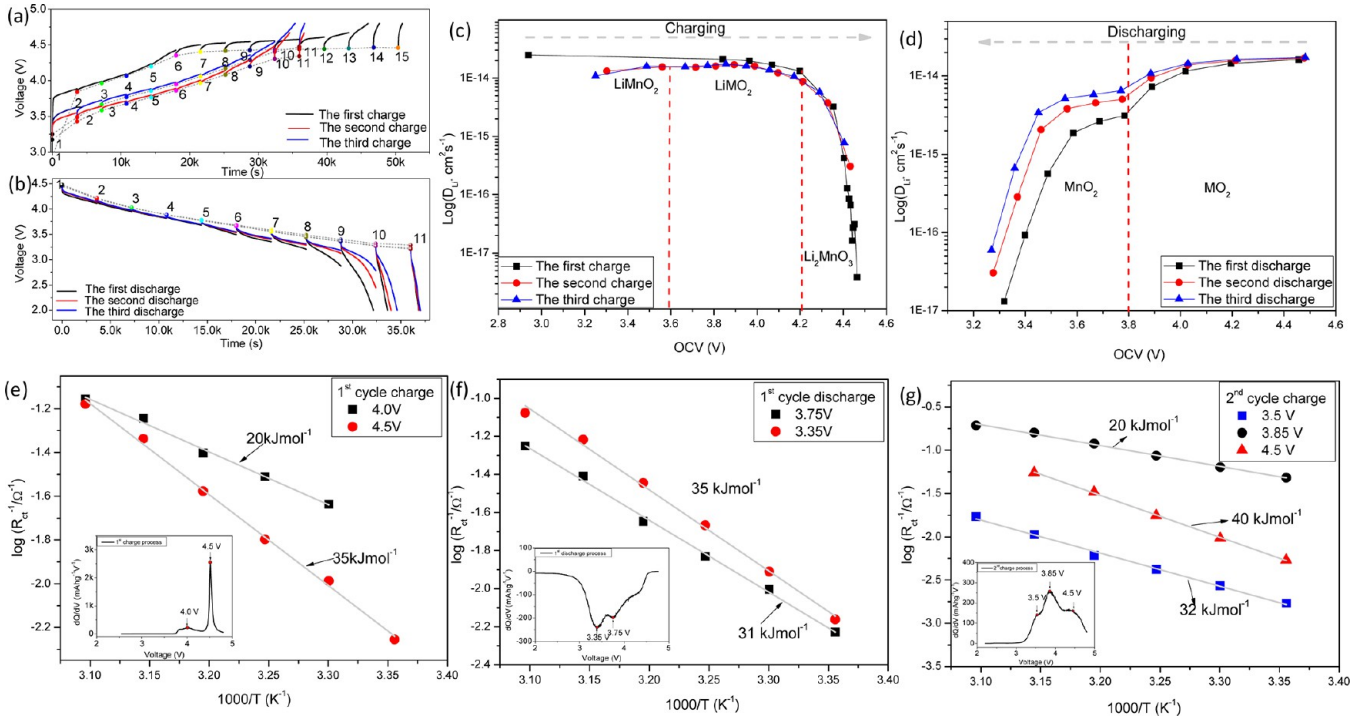

Figure 10. Galvanostatic intermittent titration technique (GITT) in the first, second, and third (a) charge and (b) discharge processes, Li^+ diffusion coefficients during the first three (c) charge and (d) discharge processes, and interface activation energy of different states during the first charge (e), discharge (f), and the second charge (g) processes of the $0.5Li_2MnO_3{\cdot}0.5LiMn_{0.42}Ni_{0.42}Co_{0.16}O_2$ electrode material. The inset figures in panels e, f, and g are the dQ/dV curves during the first charging, discharging, and second charging processes, respectively. (a) Reprinted with permission from ref 15. Copyright 2012 Royal Society of Chemistry.

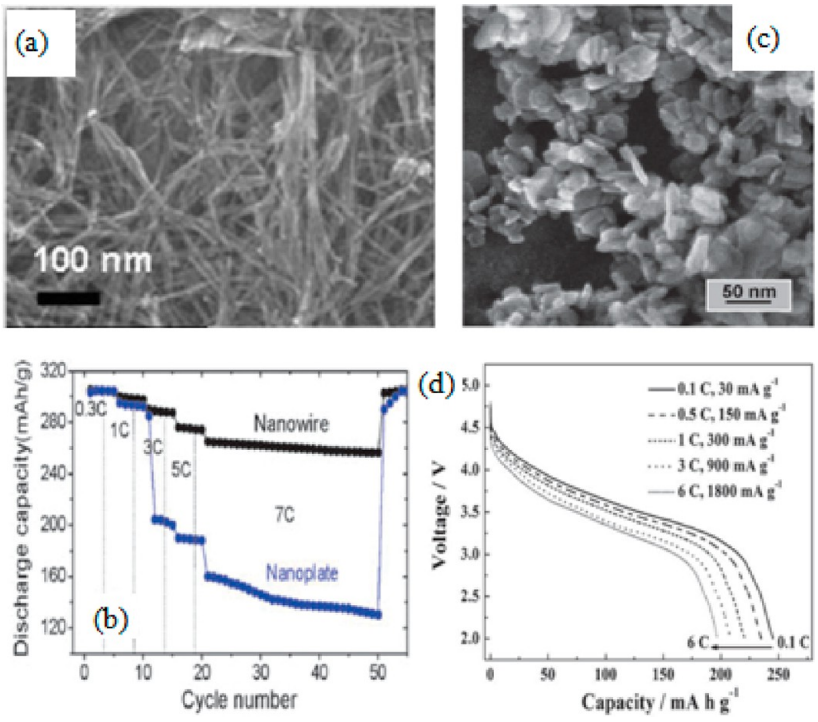

Figure 11. (a) TEM image and (b) rate capabilities of $Li[Ni_{0.25}Li_{0.15}Mn_{0.6}]O_2$ nanowires. Reprinted with permission from ref 77. Copyright 2009 Royal Society of Chemistry. (c) SEM image and (d) discharge curves with different rates (6, 3, 1, 0.5, and 0.1C) of the $Li[Li_{1/3-2x/3}Ni_xMn_{2/3-x/3}]O_2$ habit-tuned nanoplate material. Reprinted with permission from ref 78. Copyright 2010 Wiley-VCH.

oxygen arrays.[75] Thus, the voltage degradations of these LLOs during cycling are also believed to be associated with both internal and surface phase transition to a cubic spinel-like phase by the migration of transition metal ions. At present, the stepwise precycling treatment on these LLOs is used and can improve their cyclic durability.[76] The reason may be

dx.doi.org/10.1021/jz400032v | J. Phys. Chem. Lett. 2013, 4, 1268−1280

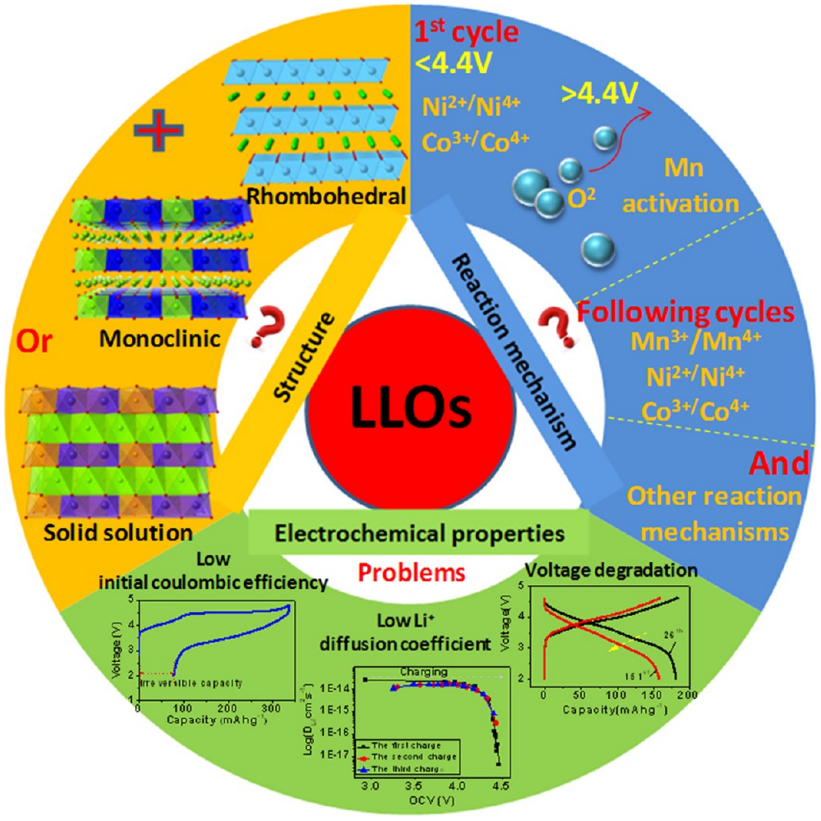

Figure 12. Current debates on structure and reaction mechanism, problems on electrochemical properties, and keys to the study in the future of Li_2MnO_3-based lithium-rich layered cathode materials.

contributed by the weakened structure damage and little structure arrangement after electrochemical cycling of these materials with this pretreatment method.

In order to reveal the kinetically controlled charge and discharge processes of these cathode materials, the lithium ion diffusion in active material and lithium ion transfer at the electrode/electrolyte interface of the LLO ($0.5Li_2MnO_3{\cdot}0.5LiMn_{0.42}Ni_{0.42}Co_{0.16}O_2$) during the first three cycles were studied in detail by means of galvanostatic intermittent titration (GITT; Figure 10a–d) and electrochemical impedance spectroscopy for interface activation energies (Figure 10e–g) methods.[15] Fifteen points in the first charge process, and 11 points in the first discharge and second and third charge/discharge processes were chosen for lithium ion diffusion coefficient calculation of this LLO (Figure 10a,b). Results show that the variation of lithium ion diffusion coefficient can be separated into two stages in all three charge and discharge processes (Figure 10c,d). On the basis of the two-phase model of this LLO, the lithium ion diffusion coefficients associated with $LiMO_2/MO_2$ ($M = Mn_{0.42}Ni_{0.42}Co_{0.16}$) components are much larger than those associated with Li_2MnO_3, $LiMnO_2/MnO_2$ components. In addition, it is also obvious that the interface activation energy associated with $LiMO_2$ (20 kJ/mol) and MO_2 (31 kJ/mol, $M = Mn_{0.42}Ni_{0.42}Co_{0.16}$) components (Figure 10e–g) is small, while that associated with Li_2MnO_3 (35 kJ/mol), $LiMnO_2$ (32 kJ/mol), and MnO_2 (35 kJ/mol) components is large. The lithium ion diffusion coefficient variations during the first three charge/discharge processes and interface activation energy variations of the electrode materials with different states, corresponding to lithium ions extraction/insertion from/into the different components and interfaces (between electrode and electrolyte) are very consistent with the two-phase models proposed and confirmed in Figure 2. Therefore, the electrochemical kinetics of the lithium ion extraction and insertion reactions in these LLOs is mainly controlled by the Li_2MnO_3 component inside these LLOs. Even though this component can be activated after the first charge process, the novel possible MnO_2 and $LiMnO_2$ components still have lower lithium ion diffusion coefficients and higher interface reaction barriers with large activation energy.

Thus, in order to improve the rate performance of these LLOs, the materials with low Li_2MnO_3 component proportion, short lithium ion diffusion pathway, and small interface reaction barrier should be introduced to these materials. Kim et al. have prepared $Li[Ni_{0.25}Li_{0.15}Mn_{0.6}]O_2$ nanowires with an aspect ratio of several hundreds and a diameter of about 30 nm (Figure 11a), exhibiting a rate capability of 95% at 4C (=1200 mA/g) (Figure 11b).[77] Meanwhile, Wei et al. have reported that a crystal habit-tuned nanoplate materials of $Li[Li_{0.17}Ni_{0.25}Mn_{0.58}]O_2$, associated with significantly increased (010) nanoplates (Figure 10 c), exhibits high rate performance (Figure 10 d).[78] Through surface modification with insulating materials (Al_2O_3 and $AlPO_4$), Manthiram et al. also found that the rate capability of these LLOs can be improved, which may be contributed to the lower charge-transfer resistance with small activation energy compared with the unmodified sample.[70] Thus, the crystal grain and particle surface modification of these LLOs are very useful to improve their rate performance.

The LLOs are very attractive for utilization as cathode materials for lithium ion batteries. Although researchers have put forth much effort in studying these materials in the past,

dx.doi.org/10.1021/jz400032v | J. Phys. Chem. Lett. 2013, 4, 1268–1280

many debates and issues over these materials still exist, and need to be clarified and solved in the future (Figure 12).

(1) The structures of these LLOs are still currently being debated (yellow region in Figure 12). The local structures are very important to the electrochemical performance, especially the rate performance of these LLOs. After synthesizing a lot of these LLOs, we found that the electrochemical properties of these LLOs were extremely sensitive to the preparation conditions and composition change, although their XRD or SXRD patterns are very similar. These phenomena may be contributed to the imperceptible variation of local structures, because the local environments govern properties such as the activation barriers, strain fields, and steric hindrances of the electrode materials, and can affect the lithium ion transport inside the electrode materials by blocking or opening the lithium ion pathways. The investigation with some novel analysis techniques, especially in situ testing methods (in situ TEM, Raman, neutron, etc.), on these LLOs will help us to reveal the more detailed nature of these LLOs, understand the reason for their sensitive electrochemical performance, and find the relationship between local structure and electrochemical properties.

(2) It is very useful to understand the reaction mechanism (blue region in Figure 12) of these materials at room temperature by the three-dimensional phase diagram. However, it is still difficult to understand the large mysterious abundant capacity of these LLOs at high temperature. The reaction mechanism of these LLOs at high temperature may be very different from that at room temperature. Some redox reactions associated with lithium ion extraction/insertion from/into some special sites may need to hurdle a larger energy barrier. The reaction mechanism of these LLOs at different environment temperatures should be focused on in the future.

(3) The electrochemical properties associated with low initial columbic efficiency, slow Li^+ diffusion speed, and voltage degradation during cycling of these LLOs are the main problems (green region in Figure 12) preventing their utilization in lithium-ion batteries. Although the surface coating with oxides, fluoride, and other resistant materials can lower the surface reactivity, provide a robust surface, and effectively improve the initial columbic efficiency, cycle stability, and rate performance of these LLOs, it cannot absolutely prevent their internal phase transformation. Thus, how to minimize the internal structure change during cycling and balance the structure variation and electrochemical performance need to be researched. Doping with some elements into the internal structure of these LLOs may be help to improve the structure stability.

In general, although there are many debates on these LLOs, they are still attractive for utilization as cathode materials in lithium ion batteries because of their large rechargeable capacities, thus, much effort with international collaboration needs to be conducted on these LLOs in the future.

AUTHOR INFORMATION

Corresponding Author

*Fax: +81-29-861-3489; Tel: 81-29-861-5795; E-mail: hs.zhou@aist.go.jp.

Notes

The authors declare no competing financial interest.

Biographies

Haijun Yu received his Ph.D. (2007) in Metallurgy Science and Engineering from the Northeastern University. In 2007-10, he worked as senior engineer at the General Research Institute for Nonferrous Metals (GRINM) in China on batteries and battery-related materials research. He is currently researching electrode materials and novel batteries for the next-generation energy storage system at the National Institute of Advanced Industrial Science and Technology (AIST), Japan.

Haoshen Zhou is now a prime senior researcher of the Energy Technology Research Institute (ETRI), National Institute of Advanced Industrial Science and Technology (AIST), and leading the Energy Interface Technology Group, ETRI, AIST, Japan. He is a guest invited professor at both The University of Tokyo and Nanjing University. His research interests include the synthesis of functional materials and their applications in lithium ion batteries, metal-air batteries, new type batteries/cells. Web page: http://unit.aist.go.jp/energy/groups/eit_e.htm

ACKNOWLEDGMENTS

This work was partially supported financially by the Funding Program for World-Leading Innovative R&D on Science and Technology (FIRST Program).

REFERENCES

(1) Tarascon, J. M.; Armand, M. Issues and Challenges Facing Rechargeable Lithium Batteries. *Nature* **2001**, *414*, 359−367.

(2) Armand, M.; Tarascon, J. M. Building Better Batteries. *Nature* **2008**, *451*, 652−657.

(3) Goodenough, J. B.; Kim, Y. Challenges for Rechargeable Li Batteries. *Chem. Mater.* **2010**, *22*, 587−603.

(4) Whittingham, M. S. Lithium Batteries and Cathode Materials. *Chem. Rev.* **2004**, *104*, 4271−4301.

(5) Etacheri, V.; Marom, R.; Elazari, R.; Salitra, G.; Aurbach, D. Challenges in the Development of Advanced Li-Ion Batteries: A Review. *Energ. Environ. Sci.* **2011**, *4*, 3243−3262.

(6) Thackeray, M. M.; Wolverton, C.; Isaacs, E. D. Electrical Energy Storage for Transportation − Approaching the Limits of, and Going Beyond, Lithium-ion Batteries. *Energ. Environ. Sci.* **2012**, *5*, 7854−7863.

(7) He, P.; Yu, H. J.; Li, D.; Zhou, H. S. Layered Lithium Transition Metal Oxide Cathodes towards High Energy Lithium-Ion Batteries. *J. Mater. Chem.* **2012**, *22*, 3680−3695.

(8) Yamada, A.; Iwane, N.; Harada, Y.; Nishimura, S.; Koyama, Y.; Tanaka, I. Lithium Iron Borates as High-Capacity Battery Electrodes. *Adv. Mater.* **2010**, *22*, 3583−3587.

(9) Nishimura, S.; Nakamura, M.; Natsui, R.; Yamada, A. New Lithium Iron Pyrophosphate as 3.5 V Class Cathode Material for Lithium Ion Battery. *J. Am. Chem. Soc.* **2010**, *132*, 13596−13597.

(10) Barpanda, P.; Ati, M.; Melot, B. C.; Rousse, G.; Chotard, J. N.; Doublet, M. L.; Sougrati, M. T.; Corr, S. A.; Jumas, J. C.; Tarascon, J. M. A 3.90 V Iron-Based Fluorosulphate Material for Lithium-Ion Batteries Crystallizing in the Triplite Structure. *Nat. Mater.* **2011**, *10*, 772−779.

(11) Thackeray, M. M.; Kang, S. H.; Johnson, C. S.; Vaughey, J. T.; Benedek, R.; Hackney, S. A. Li_2MnO_3-Stabilized $LiMO_2$ (M = Mn, Ni, Co) Electrodes for Lithium-Ion Batteries. *J. Mater. Chem.* **2007**, *17*, 3112−3125.

(12) Thackeray, M. M.; Johnson, C. S.; Vaughey, J. T.; Li, N.; Hackney, S. A. Advances in Manganese-Oxide 'Composite' Electrodes for Lithium-Ion Batteries. *J. Mater. Chem.* **2005**, *15*, 2257−2267.

(13) Yu, H. J.; Kim, H. J.; Wang, Y. R.; He, P.; Asakura, D.; Nakamura, Y.; Zhou, H. S. High-Energy 'Composite' Layered Manganese-Rich Cathode Materials via Controlling Li_2MnO_3 Phase Activation for Lithium-Ion Batteries. *Phys. Chem. Chem. Phys.* **2012**, *14*, 6584−6595.

(14) Yu, H. J.; Zhou, H. S. Initial Coulombic Efficiency Improvement of the $Li_{1.2}Mn_{0.567}Ni_{0.166}Co_{0.067}O_2$ Lithium-Rich Material by Ruthenium Substitution for Manganese. *J. Mater. Chem.* **2012**, *22*, 15507−15510.
(15) Yu, H. J.; Wang, Y. R.; Asakura, D.; Hosono, E.; Zhou, H. S. Electrochemical Kinetics of the $0.5Li_2MnO_3{\cdot}0.5LiMn_{0.42}Ni_{0.42}Co_{0.16}O_2$ 'Composite' Layered Cathode Material for Lithium-Ion Batteries. *RSC Adv.* **2012**, *2*, 8797−8807.
(16) Rossouw, M. H.; Thackeray, M. M. Lithium Manganese Oxides from Li_2MnO_3 for Rechargeable Lithium Battery Applications. *Mater. Res. Bull.* **1991**, *26*, 463−473.
(17) Rossouw, M. H.; Liles, D. C.; Thackeray, M. M. Synthesis and Structural Characterization of a Novel Layered Lithium Manganese Oxide, $Li_{0.36}Mn_{0.91}O_2$, and Its Lithiated Derivative, $Li_{1.09}Mn_{0.91}O_2$. *J. Solid State Chem.* **1993**, *104*, 464−466.
(18) Kalyani, P.; Chitra, S.; Mohan, T.; Gopukumar, S. Lithium Metal Rechargeable Cells Using Li_2MnO_3 as the Positive Electrode. *J. Power Sources* **1999**, *80*, 103−106.
(19) Ammundsen, B.; Paulsen, J. Novel Lithium-Ion Cathode Materials Based on Layered Manganese Oxides. *Adv. Mater.* **2001**, *13*, 943−956.
(20) Ammundsen, B.; Paulsen, J.; Davidson, I.; Liu, R. S.; Shen, C. H.; Chen, J. M.; Jang, L. Y.; Lee, J. F. Local Structure and First Cycle Redox Mechanism of Layered $Li_{1.2}Cr_{0.4}Mn_{0.4}O_2$ Cathode Material. *J. Electrochem. Soc.* **2002**, *149*, A431−A436.
(21) Kikkawa, J.; Akita, T.; Tabuchi, M.; Shikano, M.; Tatsumi, K.; Kohyama, M. Fe-Rich and Mn-Rich Nanodomains in $Li_{1.2}Mn_{0.4}Fe_{0.4}O_2$ Positive Electrode Materials for Lithium-Ion Batteries. *Appl. Phys. Lett.* **2007**, *91*, 054103(1)−054103(3).
(22) Kikkawa, J.; Akita, T.; Tabuchi, M.; Shikano, M.; Tatsumi, K.; Kohyama, M. Coexistence of Layered and Cubic Rocksalt Structures with a Common Oxygen Sublattice in $Li_{1.2}Mn_{0.4}Fe_{0.4}O_2$ Particles: A Transmission Electron Microscopy Study. *J. Appl. Phys.* **2008**, *103*, 104911(1)−104911(10).
(23) Kikkawa, J.; Akita, T.; Tabuchi, M.; Shikano, M.; Tatsumi, K.; Kohyama, M. Formation and Disappearance of Spinel Nanograins in $Li_{1.2-x}Mn_{0.4}Fe_{0.4}O_2$ ($0 \le x \le 0.99$) during Extraction and Insertion of Li Ions. *J. Electrochem. Soc.* **2009**, *156*, A839−A845.
(24) Kikkawa, J.; Akita, T.; Tabuchi, M.; Tatsumi, K.; Kohyama, M. Participation of Oxygen in Charge/Discharge Reactions in $Li_{1.2}Mn_{0.4}Fe_{0.4}O_2$: Evidence of Removal/Reinsertion of Oxide Ions. *J. Electrochem. Soc.* **2011**, *158*, A760−A768.
(25) Kim, J. S.; Johnson, C. S.; Vaughey, J. T.; Thackeray, M. M.; Hackney, S. A. Electrochemical and Structural Properties of $xLi_2M'O_3{\cdot}(1-x)LiMn_{0.5}Ni_{0.5}O_2$ Electrodes for Lithium Batteries (M′ = Ti, Mn, Zr; $0 \le x \le 0.3$). *Chem. Mater.* **2004**, *16*, 1996−2006.
(26) Cabana, J.; Johnson, C. S.; Yang, X. Q.; Chung, K. Y.; Yoon, W. S.; Kang, S. H.; Thackeray, M. M.; Grey, C. P. Structural Complexity of Layered-Spinel Composite Electrodes for Li-ion Batteries. *J. Mater. Res.* **2010**, *25*, 1601−1616.
(27) Pan, C. J.; Lee, Y. J.; Ammundsen, B.; Grey, C. P. Li-6 MAS NMR Studies of the Local Structure and Electrochemical Properties of Cr-Doped Lithium Manganese and Lithium Cobalt Oxide Cathode Materials for Lithium-Ion Batteries. *Chem. Mater.* **2002**, *14*, 2289−2299.
(28) Park, S. H.; Kang, S. H.; Johnson, C. S.; Amine, K.; Thackeray, M. M. Lithium-Manganese-Nickel-Oxide Electrodes with Integrated Layered-Spinel Structures for Lithium Batteries. *Electrochem. Commun.* **2007**, *9*, 262−268.
(29) Bareno, J.; Balasubramanian, M.; Kang, S. H.; Wen, J. G.; Lei, C. H.; Pol, S. V.; Petrov, I.; Abraham, D. P. Long-Range and Local Structure in the Layered Oxide $Li_{1.2}Co_{0.4}Mn_{0.4}O_2$. *Chem. Mater.* **2011**, *23*, 2039−2050.
(30) Lei, C. H.; Bareno, J.; Wen, J. G.; Petrov, I.; Kang, S. H.; Abraham, D. P. Local Structure and Composition Studies of $Li_{1.2}Ni_{0.2}Mn_{0.6}O_2$ by Analytical Electron Microscopy. *J. Power Sources* **2008**, *178*, 422−433.
(31) Bareno, J.; Lei, C. H.; Wen, J. G.; Kang, S. H.; Petrov, I.; Abraham, D. P. Local Structure of Layered Oxide Electrode Materials for Lithium-Ion Batteries. *Adv. Mater.* **2010**, *22*, 1122−1127.
(32) Gu, M.; Belharouak, I.; Genc, A.; Wang, Z. G.; Wang, D. P.; Amine, K.; Gao, F.; Zhou, G. W.; Thevuthasan, S.; Baer, D. R.; et al. Conflicting Roles of Nickel in Controlling Cathode Performance in Lithium Ion Batteries. *Nano Lett.* **2012**, *12*, 5186−5191.
(33) Boulineau, A.; Simonin, L.; Colin, J. F.; Canevet, E.; Daniel, L.; Patoux, S. Evolutions of $Li_{1.2}Mn_{0.61}Ni_{0.18}Mg_{0.01}O_2$ during the Initial Charge/Discharge Cycle Studied by Advanced Electron Microscopy. *Chem. Mater.* **2012**, *24*, 3558−3566.
(34) Xu, B.; Fell, C. R.; Chi, M. F.; Meng, Y. S. Identifying Surface Structural Changes in Layered Li-Excess Nickel Manganese Oxides in High Voltage Lithium Ion Batteries: A Joint Experimental and Theoretical Study. *Energ. Environ. Sci.* **2011**, *4*, 2223−2233.
(35) Koga, H.; Croguennec, L.; Mannessiez, P.; Menetrier, M.; Weill, F.; Bourgeois, L.; Duttine, M.; Suard, E.; Delmas, C. $Li_{1.20}Mn_{0.54}Co_{0.13}Ni_{0.13}O_2$ with Different Particle Sizes as Attractive Positive Electrode Materials for Lithium-Ion Batteries: Insights into Their Structure. *J. Phys. Chem. C* **2012**, *116*, 13497−13506.
(36) Wen, J. G.; Bareno, J.; Lei, C. H.; Kang, S. H.; Balasubramanian, M.; Petrov, I.; Abraham, D. P. Analytical Electron Microscopy of $Li_{1.2}Co_{0.4}Mn_{0.4}O_2$ for Lithium-Ion Batteries. *Solid State Ionics* **2011**, *182*, 98−107.
(37) Jarvis, K. A.; Deng, Z. Q.; Allard, L. F.; Manthiram, A.; Ferreira, P. J. Atomic Structure of a Lithium-Rich Layered Oxide Material for Lithium-Ion Batteries: Evidence of A Solid Solution. *Chem. Mater.* **2011**, *23*, 3614−3621.
(38) Yoon, W. S.; Kim, N.; Yang, X. Q.; McBreen, J.; Grey, C. P. Li-6 MAS NMR and in Situ X-Ray Studies of Lithium Nickel Manganese Oxides. *J. Power Sources* **2003**, *119*, 649−653.
(39) Breger, J.; Jiang, M.; Dupre, N.; Meng, Y. S.; Shao-Horn, Y.; Ceder, G.; Grey, C. P. High-Resolution X-ray Diffraction, DIFFaX, NMR and First Principles Study of Disorder in the Li_2MnO_3-$Li[Ni_{1/2}Mn_{1/2}]O_2$ Solid Solution. *J. Solid State Chem.* **2005**, *178*, 2575−2585.
(40) Ohzuku, T.; Nagayama, M.; Tsuji, K.; Ariyoshi, K. High-Capacity Lithium Insertion Materials of Lithium Nickel Manganese Oxides for Advanced Lithium-ion Batteries: Toward Rechargeable Capacity More Than 300 mA h g^{-1}. *J. Mater. Chem.* **2011**, *21*, 10179−10188.
(41) Thackeray, M. M.; Kang, S. H.; Johnson, C. S.; Vaughey, J. T.; Hackney, S. A. Comments on the Structural Complexity of Lithium-Rich $Li_{1+x}M_{1-x}O_2$ Electrodes (M = Mn, Ni, Co) for Lithium Batteries. *Electrochem. Commun.* **2006**, *8*, 1531−1538.
(42) Kang, S. H.; Kempgens, P.; Greenbaum, S.; Kropf, A. J.; Amine, K.; Thackeray, M. M. Interpreting the Structural and Electrochemical Complexity of $0.5Li_2MnO_3{\cdot}0.5LiMO_2$ Electrodes for Lithium Batteries (M = $Mn_{0.5-x}Ni_{0.5-x}Co_{2x}$, $0 \le x \le 0.5$). *J. Mater. Chem.* **2007**, *17*, 2069−2077.
(43) Kikkawa, J.; Akita, T.; Tabuchi, M.; Shikano, M.; Tatsumi, K.; Kohyama, M. Real-Space Observation of Li Extraction/Insertion in $Li_{1.2}Mn_{0.4}Fe_{0.4}O_2$ Positive Electrode Material for Li-Ion Batteries. *Electrochem. Solid-State Lett.* **2008**, *11*, A183−A186.
(44) Grinberg, I.; Cooper, V. R.; Rappe, A. M. Relationship Between Local Structure and Phase Transitions of A Disordered Solid Solution. *Nature* **2002**, *419*, 909−911.
(45) Frenkel, A.; Stern, E. A.; Voronel, A.; Qian, M.; Newville, M. Buckled Crystalline-Structure of Mixed Ionic Salts. *Phys. Rev. Lett.* **1993**, *71*, 3485−3488.
(46) Lei, C. H.; Wen, J. G.; Sardela, M.; Bareno, J.; Petrov, I.; Kang, S. H.; Abraham, D. P. Structural Study of Li_2MnO_3 by Electron Microscopy. *J. Mater. Sci.* **2009**, *44*, 5579−5587.
(47) Rossen, E.; Jones, C. D. W.; Dahn, J. R. Structure and Electrochemistry of $Li_xMn_yNi_{1-y}O_2$. *Solid State Ionics* **1992**, *57*, 311−318.
(48) Lu, Z. H.; MacNeil, D. D.; Dahn, J. R. Layered Cathode Materials $Li[Ni_xLi_{1/3-2x/3}Mn_{2/3-x/3}]O_2$ for Lithium-Ion Batteries. *Electrochem. Solid-State Lett.* **2001**, *4*, A191−A194.

(49) Lu, Z. H.; Beaulieu, L. Y.; Donaberger, R. A.; Thomas, C. L.; Dahn, J. R. Synthesis, Structure, and Electrochemical Behavior of $Li[Ni_xLi_{1/3-2x/3}Mn_{2/3-x/3}]O_2$. *J. Electrochem. Soc.* **2002**, *149*, A778−A791.
(50) Yabuuchi, N.; Yoshii, K.; Myung, S. T.; Nakai, I.; Komaba, S. Detailed Studies of a High-Capacity Electrode Material for Rechargeable Batteries, Li_2MnO_3−$LiCo_{1/3}Ni_{1/3}Mn_{1/3}O_2$. *J. Am. Chem. Soc.* **2011**, *133*, 4404−4419.
(51) Johnson, C. S.; Kim, J. S.; Lefief, C.; Li, N.; Vaughey, J. T.; Thackeray, M. M. The Significance of the Li_2MnO_3 Component in 'Composite' $xLi_2MnO_3{\cdot}(1-x)LiMn_{0.5}Ni_{0.5}O_2$ Electrodes. *Electrochem. Commun.* **2004**, *6*, 1085−1091.
(52) Armstrong, A. R.; Holzapfel, M.; Novak, P.; Johnson, C. S.; Kang, S. H.; Thackeray, M. M.; Bruce, P. G. Demonstrating Oxygen Loss and Associated Structural Reorganization in the Lithium Battery Cathode $Li[Ni_{0.2}Li_{0.2}Mn_{0.6}]O_2$. *J. Am. Chem. Soc.* **2006**, *128*, 8694−8698.
(53) Kang, S. H.; Johnson, C. S.; Vaughey, J. T.; Amine, K.; Thackeray, M. M. The Effects of Acid Treatment on the Electrochemical Properties of $0.5Li_2MnO_3{\cdot}0.5LiNi_{0.44}Co_{0.25}Mn_{0.31}O_2$ Electrodes in Lithium Cells. *J. Electrochem. Soc.* **2006**, *153*, A1186−A1192.
(54) Johnson, C. S.; Li, N. C.; Lefief, C.; Thackeray, M. M. Anomalous Capacity and Cycling Stability of $xLi_2MnO_3{\cdot}(1-x)LiMO_2$ Electrodes (M = Mn, Ni, Co) in Lithium Batteries at 50 °C. *Electrochem. Commun.* **2007**, *9*, 787−795.
(55) Hy, S.; Su, W. N.; Chen, J. M.; Hwang, B. J. Soft X-ray Absorption Spectroscopic and Raman Studies on $Li_{1.2}Ni_{0.2}Mn_{0.6}O_2$ for Lithium-Ion Batteries. *J. Phys. Chem. C* **2012**, *116*, 25242−25247.
(56) Lu, Z. H.; Dahn, J. R. Understanding the Anomalous Capacity of $Li/Li[Ni_xLi_{(1/3-2x/3)}Mn_{(2/3-x/3)}]O_2$ Cells Using in Situ X-ray Diffraction and Electrochemical Studies. *J. Electrochem. Soc.* **2002**, *149*, A815−A822.
(57) Simonin, L.; Colin, J. F.; Ranieri, V.; Canevet, E.; Martin, J. F.; Bourbon, C.; Baehtz, C.; Strobel, P.; Daniel, L.; Patoux, S. In Situ Investigations of A Li-Rich Mn-Ni Layered Oxide for Li-Ion Batteries. *J. Mater. Chem.* **2012**, *22*, 11316−11322.
(58) Jiang, M.; Key, B.; Meng, Y. S.; Grey, C. P. Electrochemical and Structural Study of the Layered, "Li-Excess" Lithium-Ion Battery Electrode Material $Li[Li_{1/9}Ni_{1/3}Mn_{5/9}]O_2$. *Chem. Mater.* **2009**, *21*, 2733−2745.
(59) Johnson, C. S.; Li, N. C.; Lefief, C.; Vaughey, J. T.; Thackeray, M. M. Synthesis, Characterization and Electrochemistry of Lithium Battery Electrodes: $xLi_2MnO_3{\cdot}(1-x)LiMn_{0.333}Ni_{0.333}Co_{0.333}O_2$ ($0 \le x \le 0.7$). *Chem. Mater.* **2008**, *20*, 6095−6106.
(60) Amalraj, F.; Kovacheva, D.; Talianker, M.; Zeiri, L.; Grinblat, J.; Leifer, N.; Goobes, G.; Markovsky, B.; Aurbach, D. Synthesis of Integrated Cathode Materials $xLi_2MnO_3{\cdot}(1-x)LiMn_{1/3}Ni_{1/3}Co_{1/3}O_2$ (x = 0.3, 0.5, 0.7) and Studies of Their Electrochemical Behavior. *J. Electrochem. Soc.* **2010**, *157*, A1121−A1130.
(61) Zheng, J. M.; Wu, X. B.; Yang, Y. A Comparison of Preparation Method on the Electrochemical Performance of Cathode Material $Li[Li_{0.2}Mn_{0.54}Ni_{0.13}Co_{0.13}]O_2$ for Lithium Ion Battery. *Electrochim. Acta* **2011**, *56*, 3071−3078.
(62) Van Bommel, A.; Dahn, J. R. Kinetics Study of the High Potential Range of Lithium-Rich Transition-Metal Oxides for Lithium-Ion Batteries by Electrochemical Methods. *Electrochem. Solid-State Lett.* **2010**, *13*, A62−A64.
(63) Lim, J. H.; Bang, H.; Lee, K. S.; Amine, K.; Sun, Y. K. Electrochemical Characterization of Li_2MnO_3−$Li[Ni_{1/3}Co_{1/3}Mn_{1/3}]O_2$−$LiNiO_2$ Cathode Synthesized via Co-precipitation for Lithium Secondary Batteries. *J. Power Sources* **2009**, *189*, 571−575.
(64) Mangani, I. R.; Park, C. W.; Yoon, Y. K.; Beom, J. H.; Kim, J. Synthesis and Characterization of $Li[Li_{0.27}Cr_{0.15}Al_{0.05}Mn_{0.53}]O_2$ Cathode for Lithium-Ion Batteries. *J. Electrochem. Soc.* **2007**, *154*, A359−A363.
(65) Park, C. W.; Kim, S. H.; Mangani, I. R.; Lee, J. H.; Boo, S.; Kim, J. Synthesis and Materials Characterization of Li_2MnO_3-$LiCrO_2$ System Nanocomposite Electrode Materials. *Mater. Res. Bull.* **2007**, *42*, 1374−1383.
(66) Tabuchi, M.; Nakashima, A.; Ado, K.; Sakaebe, H.; Kobayashi, H.; Kageyama, H.; Tatsumi, K.; Kobayashi, Y.; Seki, S.; Yamanaka, A. The Effects of Preparation Condition and Dopant on the Electrochemical Property for Fe-Substituted Li_2MnO_3. *J. Power Sources* **2005**, *146*, 287−293.
(67) Tabuchi, M.; Nakashima, A.; Ado, K.; Kageyarna, H.; Tatsumi, K. Heat-Treatment Effect on Phase Stability, Cation Distribution, Chemical Composition, and Electrochemical Behavior for Fe-Substituted Li_2MnO_3. *Chem. Mater.* **2005**, *17*, 4668−4677.
(68) Van Bommel, A.; Krause, L. J.; Dahn, J. R. Investigation of the Irreversible Capacity Loss in the Lithium-Rich Oxide $Li-[Li_{1/5}Ni_{1/5}Mn_{3/5}]O_2$. *J. Electrochem. Soc.* **2011**, *158*, A731−A735.
(69) Kang, S. H.; Thackeray, M. M. Stabilization of $xLi_2MnO_3{\cdot}(1-x)LiMO_2$ Electrode Surfaces (M = Mn, Ni, Co) with Mildly Acidic, Fluorinated Solutions. *J. Electrochem. Soc.* **2008**, *155*, A269−A275.
(70) Manthiram, A. Materials Challenges and Opportunities of Lithium Ion Batteries. *J. Phys. Chem. Lett.* **2011**, *2*, 176−184.
(71) Croy, J. R.; Kim, D.; Balasubramanian, M.; Gallagher, K.; Kang, S. H.; Thackeray, M. M. Countering the Voltage Decay in High Capacity $xLi_2MnO_3{\cdot}(1-x)LiMO_2$ Electrodes (M = Mn, Ni, Co) for Li^+ Ion Batteries. *J. Electrochem. Soc.* **2012**, *159*, A781−A790.
(72) Song, B. H.; Liu, Z. W.; Lai, M. O.; Lu, L. Structural Evolution and the Capacity Fade Mechanism upon Long-Term Cycling in Li-Rich Cathode Material. *Phys. Chem. Chem. Phys.* **2012**, *14*, 12875−12883.
(73) Wu, Y.; Manthiram, A. High Capacity, Surface-Modified Layered $Li[Li_{(1-x)/3}Mn_{(2-x)/3}Ni_{x/3}Co_{x/3}]O_2$ Cathodes with Low Irreversible Capacity Loss. *Electrochem. Solid-State Lett.* **2006**, *9*, A221−A224.
(74) Shin, D.; Wolverton, C.; Croy, J. R.; Balasubramanian, M.; Kang, S. H.; Rivera, C. M. L.; Thackeray, M. M. First-Principles Calculations, Electrochemical and X-ray Absorption Studies of Li-Ni-PO_4 Surface-Treated $xLi_2MnO_3{\cdot}(1-x)LiMO_2$ (M = Mn, Ni, Co) Electrodes for Li-Ion Batteries. *J. Electrochem. Soc.* **2012**, *159*, A121−A127.
(75) Reed, J.; Ceder, G.; Van der Ven, A. Layered-to-Spinel Phase Transition in Li_xMnO_2. *Electrochem. Solid-State Lett.* **2001**, *4*, A78−A81.
(76) Ito, A.; Li, D. C.; Sato, Y.; Arao, M.; Watanabe, M.; Hatano, M.; Horie, H.; Ohsawa, Y. Cyclic Deterioration and Its Improvement for Li-Rich Layered Cathode Material $Li[Ni_{0.17}Li_{0.2}Co_{0.07}Mn_{0.56}]O_2$. *J. Power Sources* **2010**, *195*, 567−573.
(77) Kim, M. G.; Jo, M.; Hong, Y. S.; Cho, J. Template-Free Synthesis of $Li[Ni_{0.25}Li_{0.15}Mn_{0.6}]O_{-2}$ Nanowires for High Performance Lithium Battery Cathode. *Chem. Commun.* **2009**, 218−220.
(78) Wei, G. Z.; Lu, X.; Ke, F. S.; Huang, L.; Li, J. T.; Wang, Z. X.; Zhou, Z. Y.; Sun, S. G. Crystal Habit-Tuned Nanoplate Material of $Li[Li_{1/3-2x/3}Ni_xMn_{2/3-x/3}]O_2$ for High-Rate Performance Lithium-Ion Batteries. *Adv. Mater.* **2010**, *22*, 4364−4367.